Supplement of The Cryosphere, 17, 3739–3759, 2023
https://doi.org/10.5194/tc-17-3739-2023-supplement

The Cryosphere Open Access EGU

Supplement of

The stability of present-day Antarctic grounding lines – Part 1: No indication of marine ice sheet instability in the current geometry

Emily A. Hill et al.

Correspondence to: Olivier Gagliardini (olivier.gagliardini@univ-grenoble-alpes.fr)

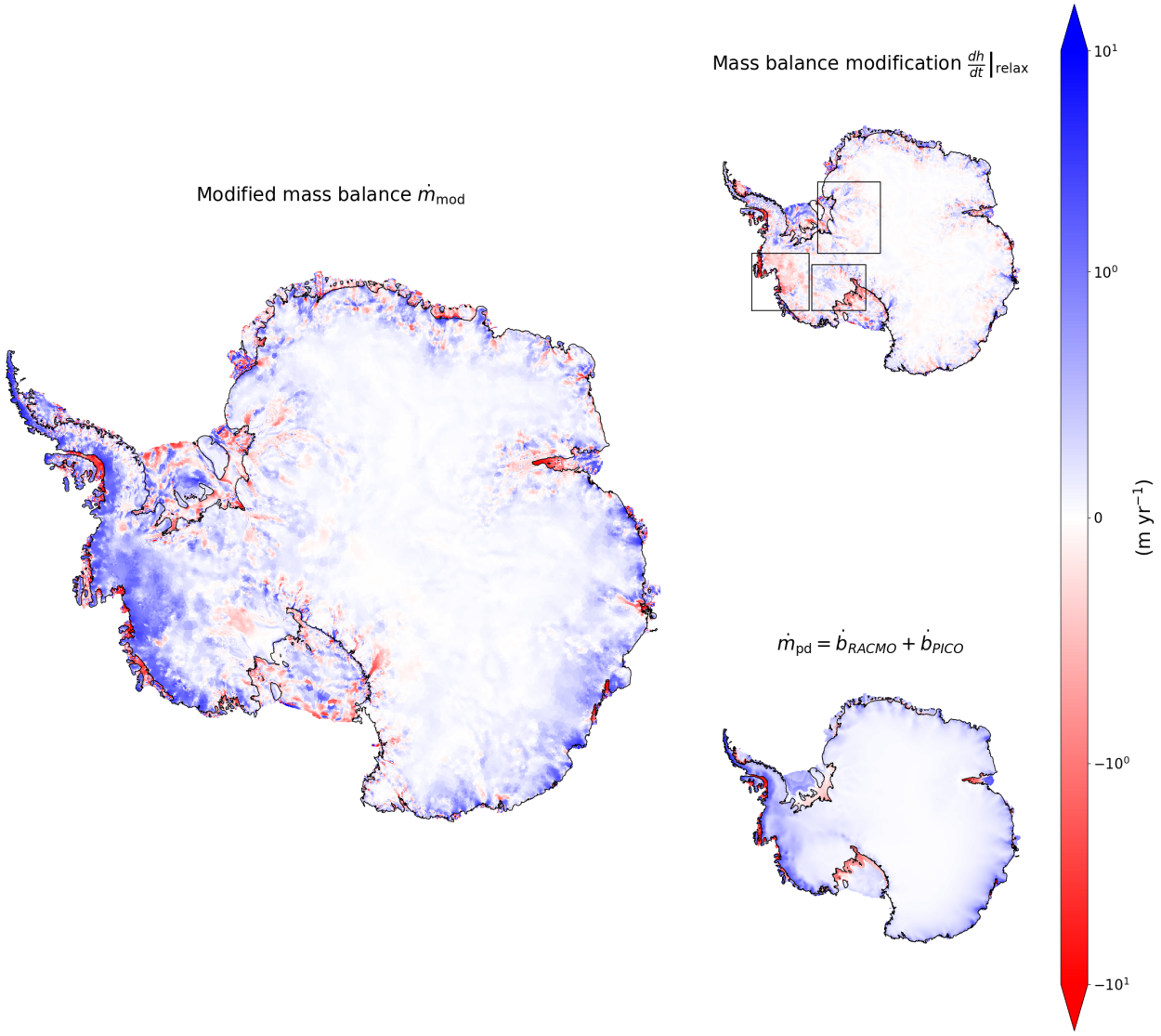

Figure S1. Modified mass balance terms in Eq. (1) for Elmer/Ice. Left, modified mass balance field $\dot{m}_{\mathrm{mod}}$ used in the forward experiments. Top right, modification term $dh/dt|_{\mathrm{relax}}$ applied to achieve a model steady state. Black boxes highlight the regions shown in Fig. S3. Bottom right, the present-day mass balance $\dot{m}_{\mathrm{pd}}$ as represented by RACMO and PICO.

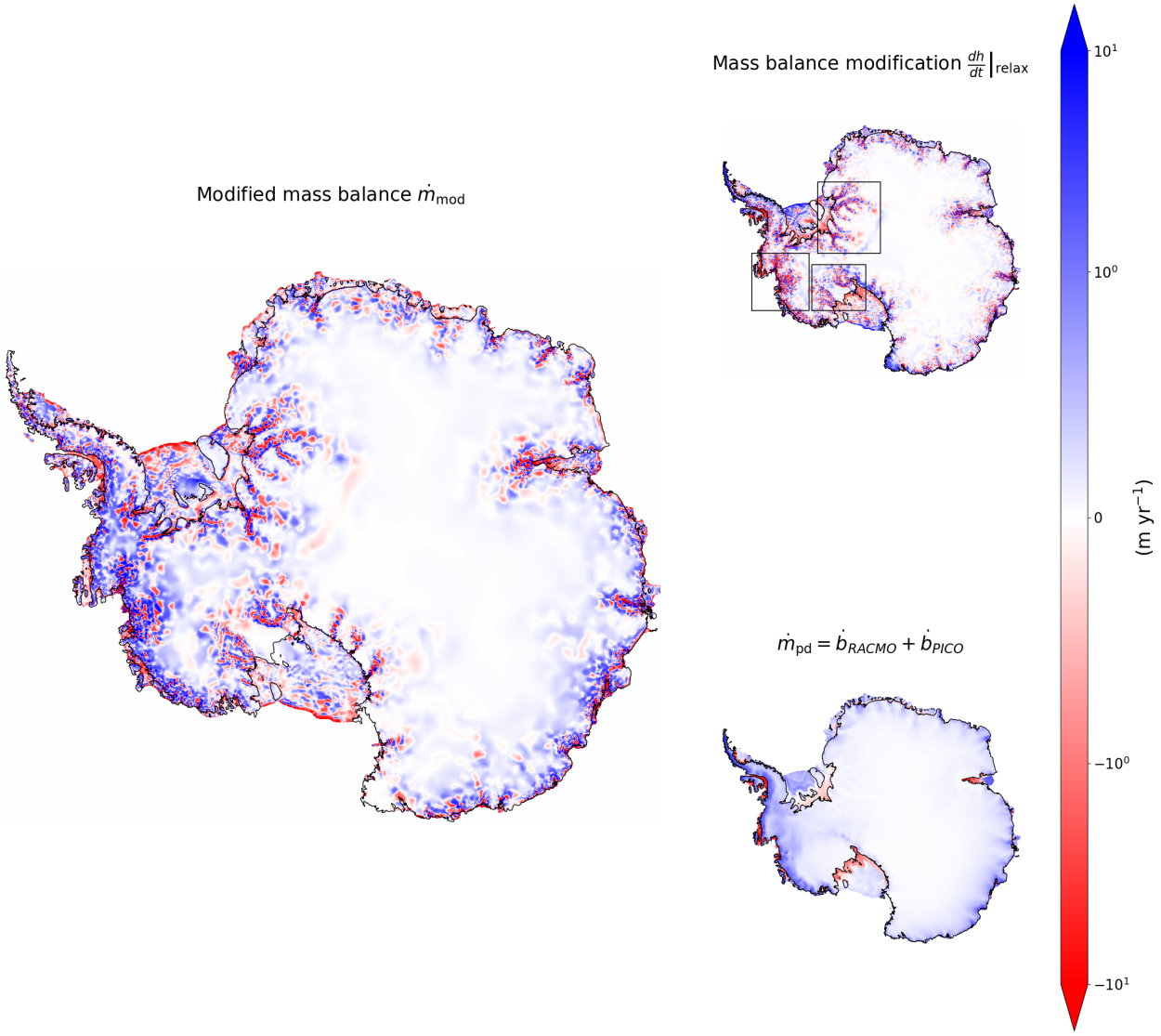

Figure S2. Modified mass balance terms in Eq. (1) for Úa. Left, modified mass balance field $\dot{m}_{\mathrm{mod}}$ used in the forward experiments. Top right, modification term $dh/dt|_{\mathrm{relax}}$ applied to achieve a model steady state. Black boxes highlight the regions shown in Fig. S3. Bottom right, the present-day mass balance $\dot{m}_{\mathrm{pd}}$ as represented by RACMO and PICO.

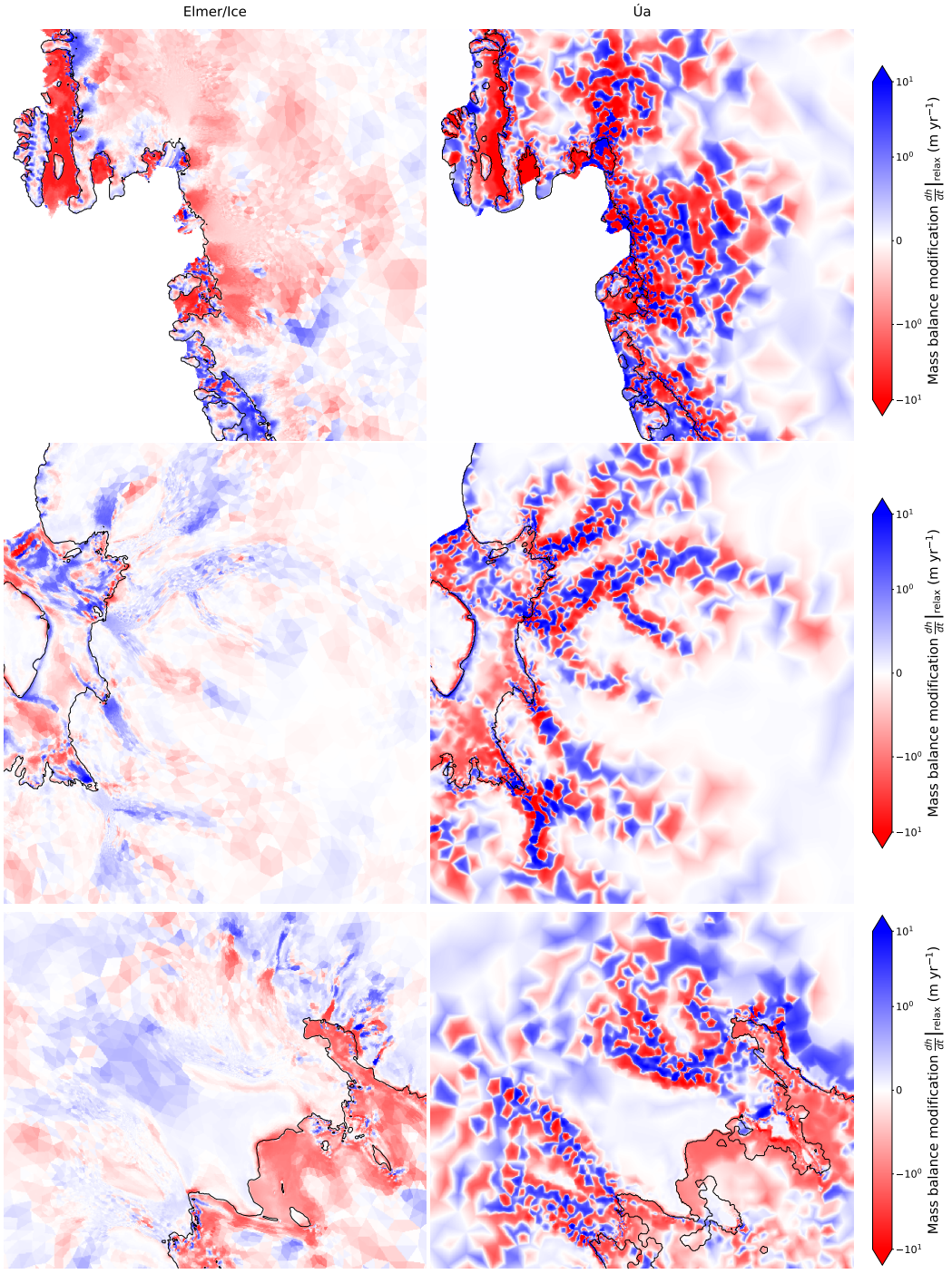

Figure S3. Regional maps of the mass balance modification terms (see Figs. S1 and S2 for full maps) used in Elmer/Ice and Úa. The top two panels show the Amundsen Sea Embayment region in West Antarctica, the middle panels show the glaciers draining into the Filchner Ice Shelf and the bottom panels show ice streams of the Siple Coast feeding the central part of the Ross Ice Shelf.

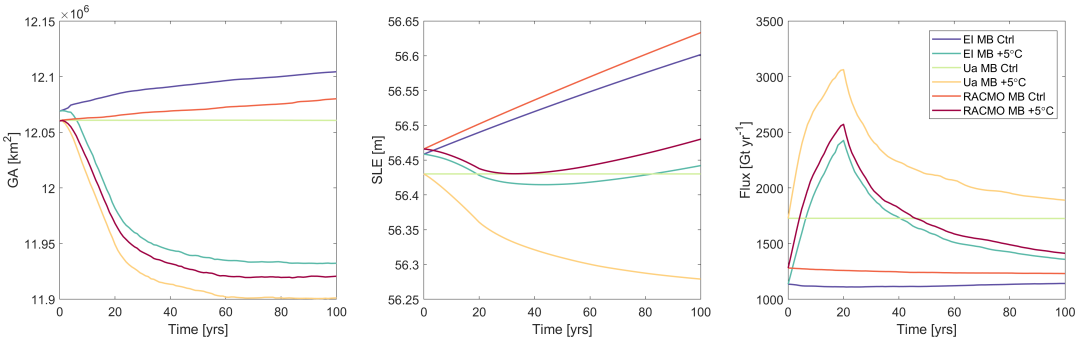

Figure S4. Numerical experiments using Úa where the unperturbed reference/control run is either in steady state ("Ua MB") or a transient state (i.e. drifting with time) using either 1) the modified mass balance field from Elmer/Ice ("EI MB") or 2) the RACMO+PICO mass balance ("RACMO MB"). Left panel shows grounded area (GA) in km^2, middle shows sea level equivalent (SLE) ice volume in m and right shows the flux calculated across the grounding line in Gt yr^{-1}. The perturbed experiments (using a 5 °C perturbation) are shown for all three runs. In all cases the variables begin to return back to their initial (i.e. unperturbed) values.

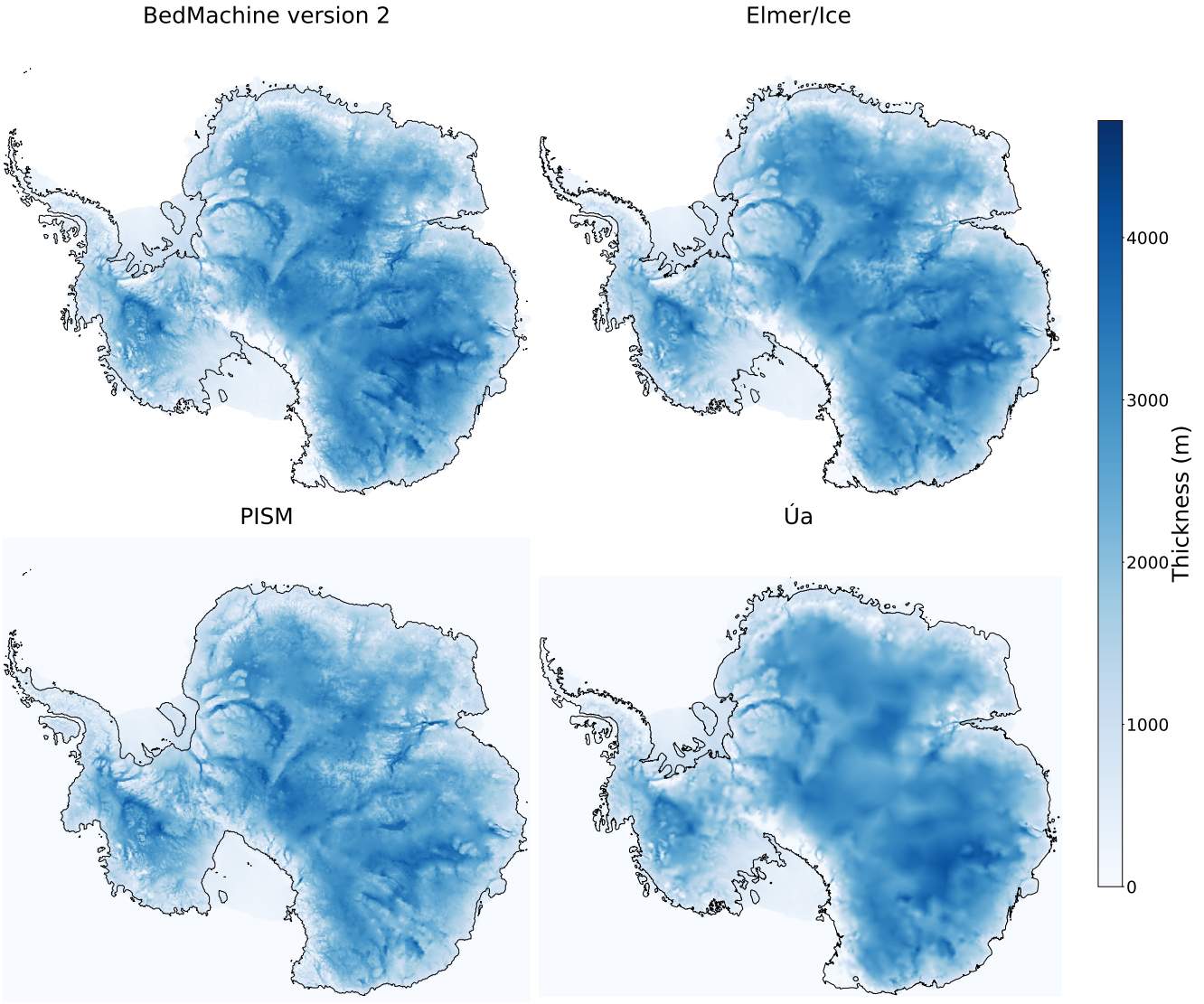

Figure S5. Ice thickness from BedMachine Antarctica and ice thickness calculated in each ice sheet model after initialisation. Grounding lines are shown in black.

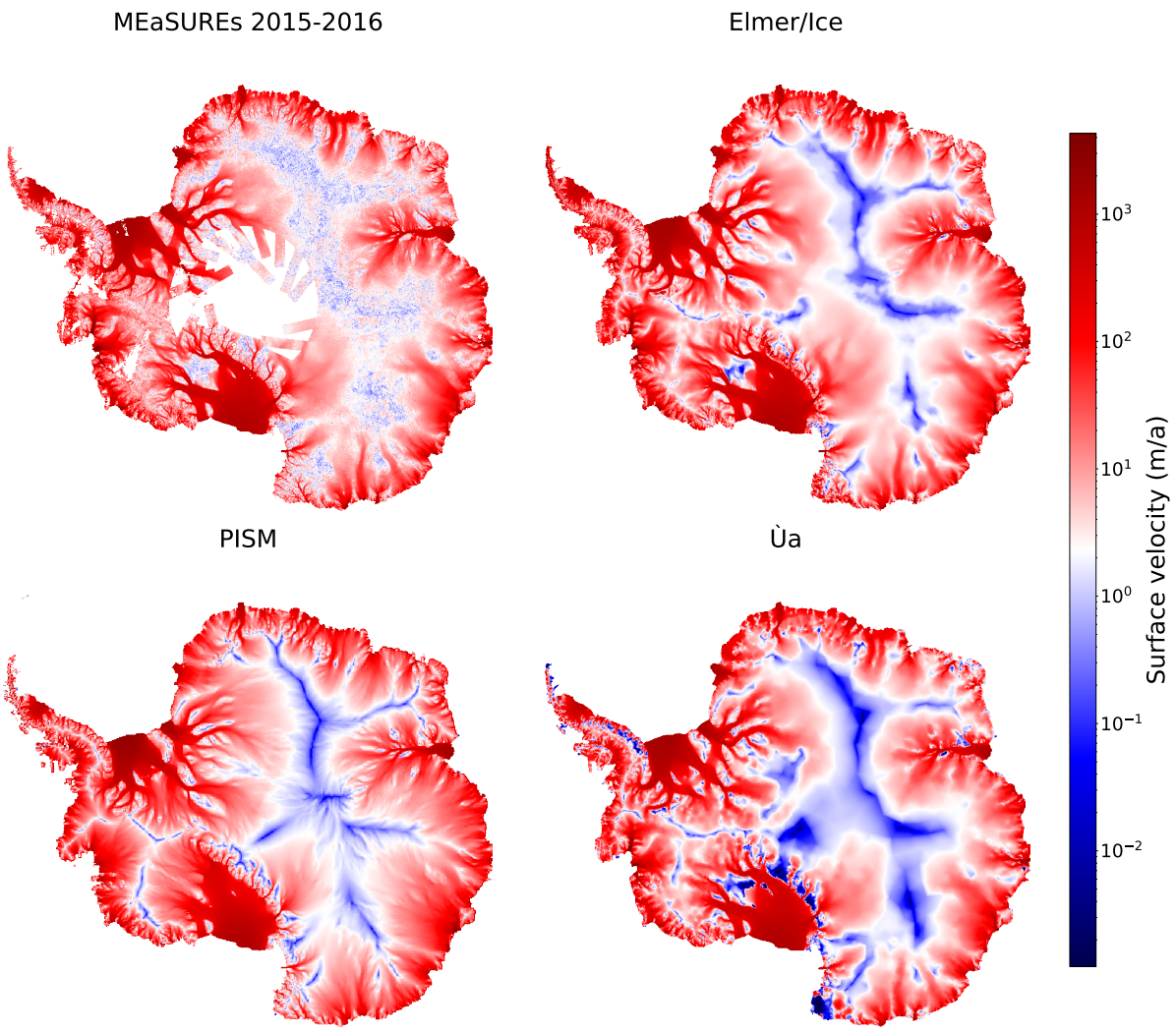

Figure S6. Annual ice surface velocities from MEaSUREs for 2015/16 and ice surface velocities calculated in each ice sheet model after initialisation.

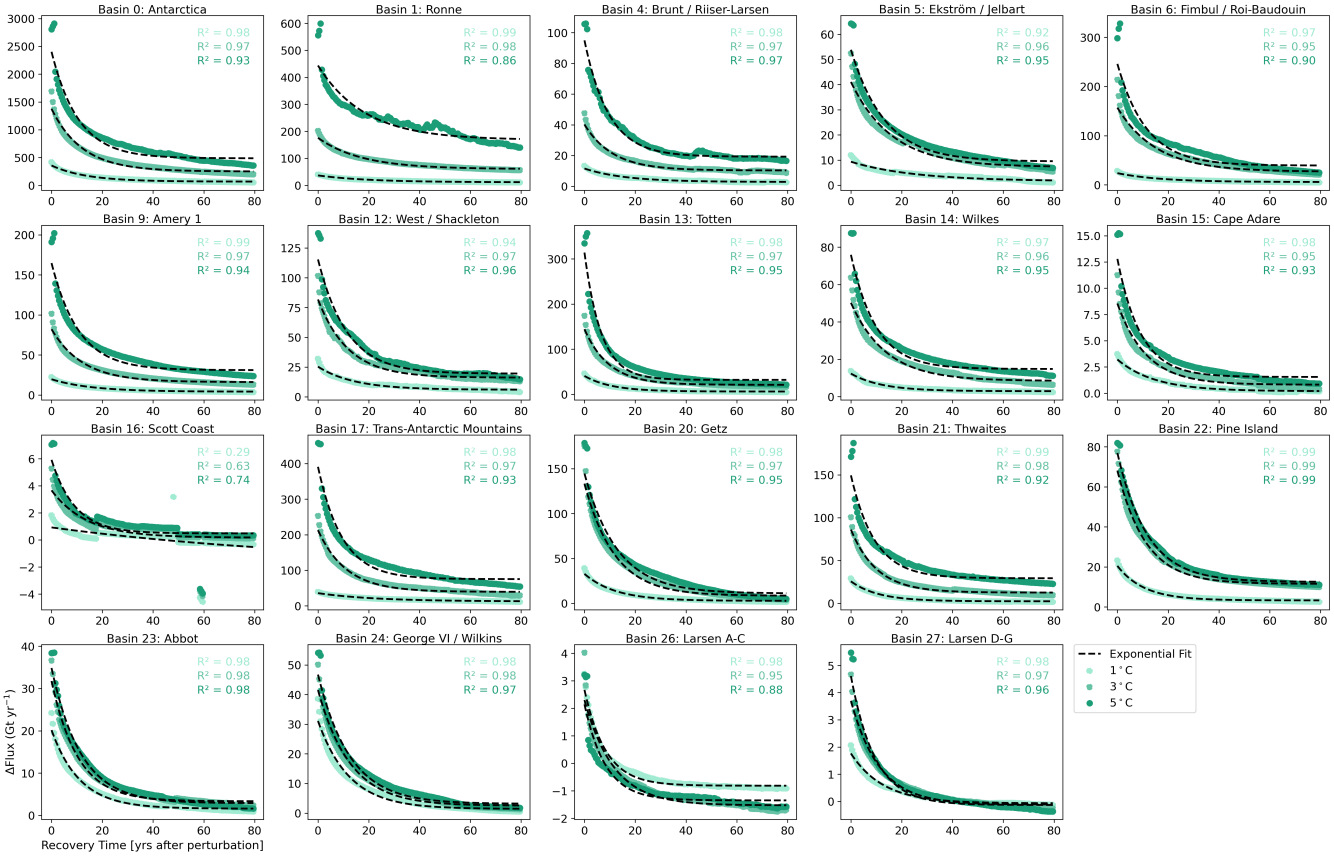

Figure S7. Exponential recovery of the change in ice flux across the grounding line in the 80 years after the perturbation. Results are presented by drainage basin for perturbation experiments using Elmer/Ice. In each case the coloured points are the model results for each perturbation experiment and the dashed lines are the exponential fit. R^2 values are shown for each experiment in the corresponding colour.

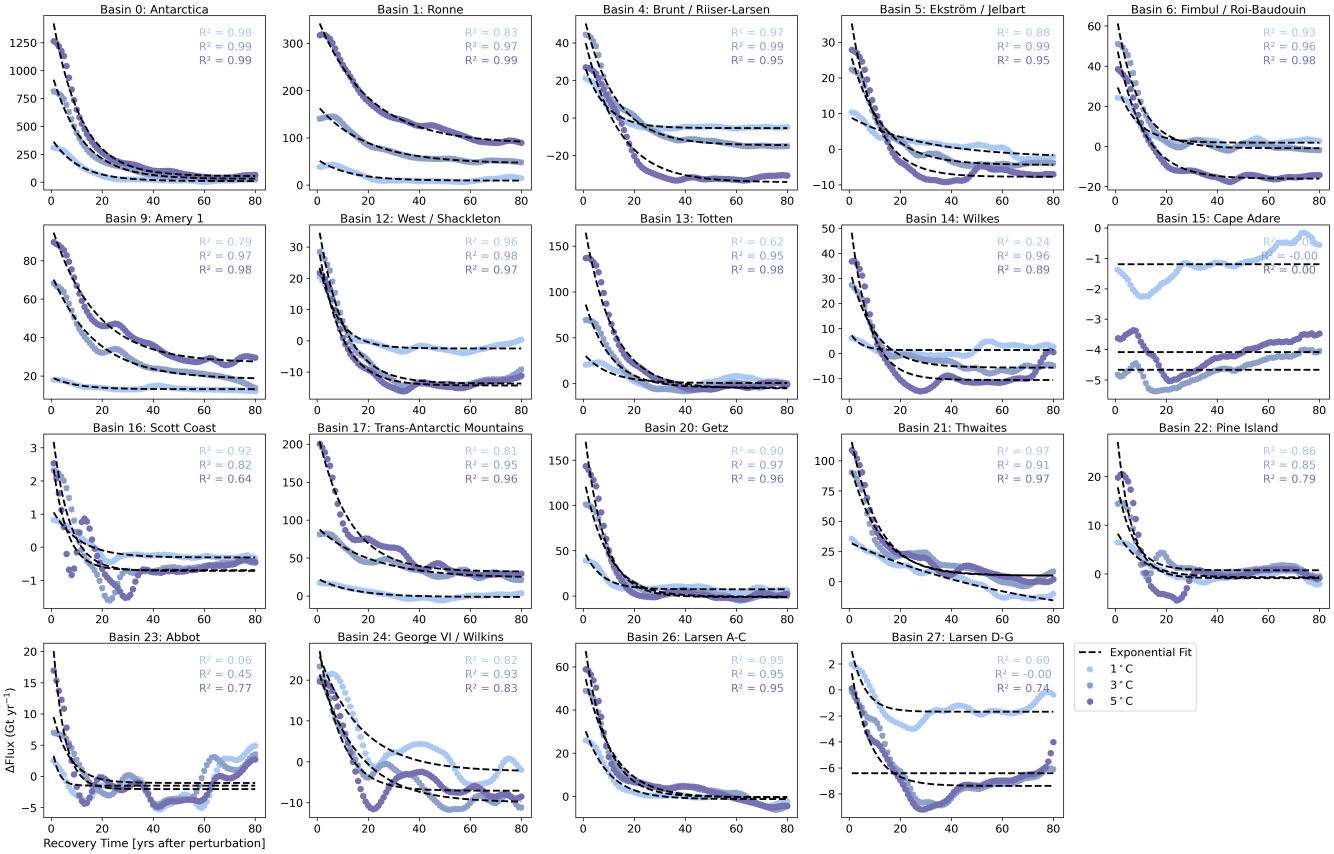

Figure S8. Exponential recovery of the change in ice flux across the grounding line in the 80 years after the perturbation. Results are presented by drainage basin for perturbation experiments using PISM. In each case the coloured points are the model results for each perturbation experiment and the dashed lines are the exponential fit. R^2 values are shown for each experiment in the corresponding colour.

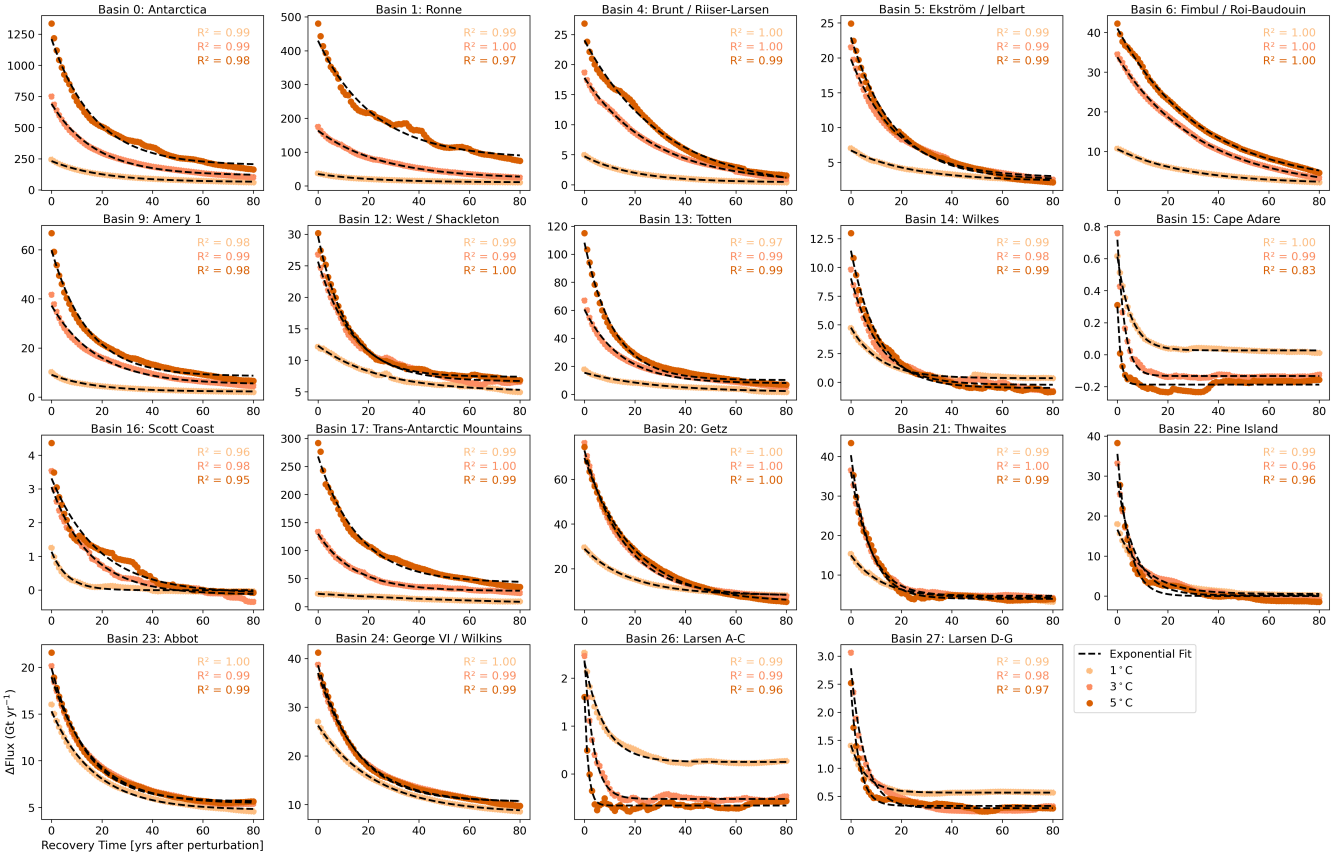

Figure S9. Exponential recovery of the change in ice flux across the grounding line in the 80 years after the perturbation. Results are presented by drainage basin for perturbation experiments using Úa. In each case the coloured points are the model results for each perturbation experiment and the dashed lines are the exponential fit. R^2 values are shown for each experiment in the corresponding colour.

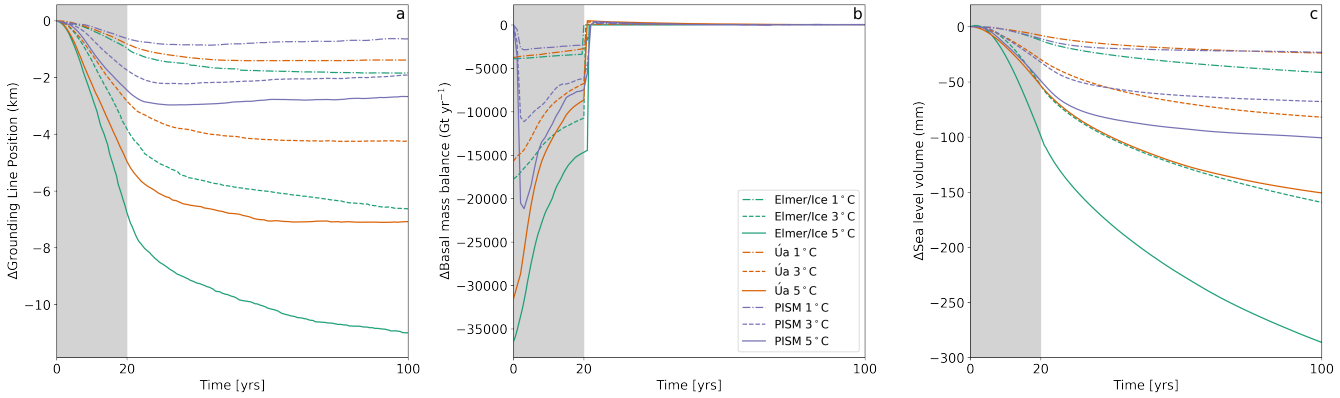

Figure S10. Additional Antarctic-wide results. Change in grounding line position, change in total basal mass balance and change in sea level volume are shown for all three models and all perturbation experiments with respect to their control experiments.

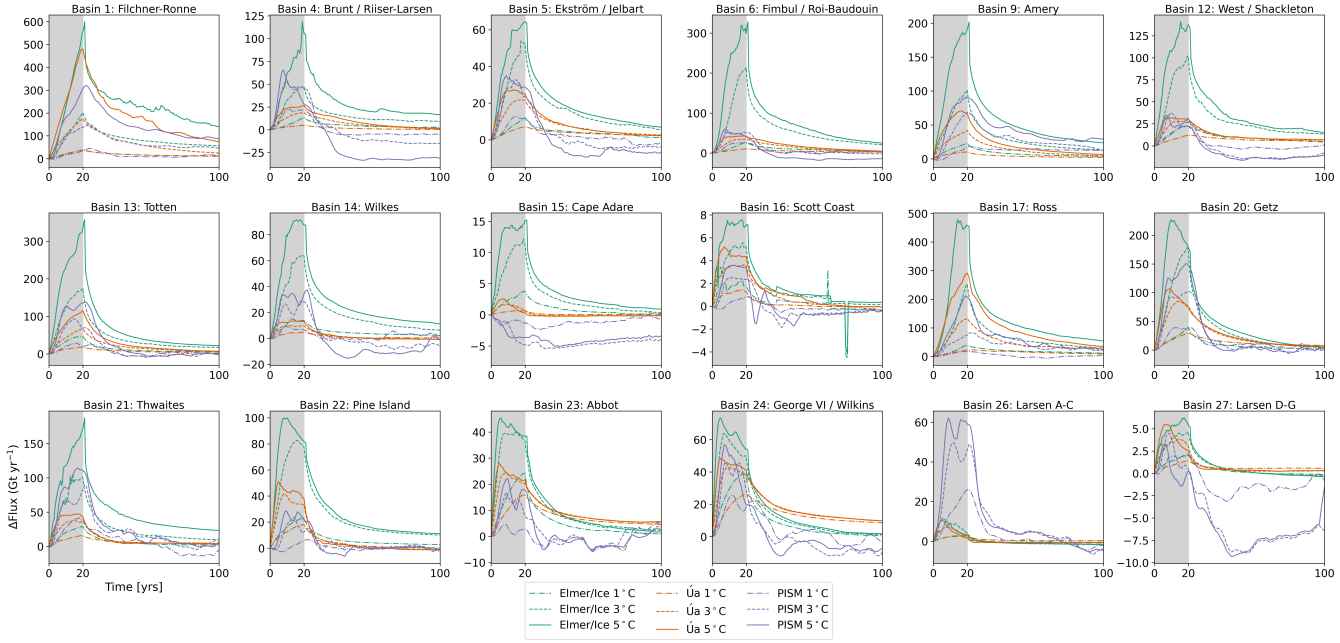

Figure S11. Change in grounding line flux for individual drainage basins. Results are shown for all three models and all perturbation experiments with respect to their control experiments.

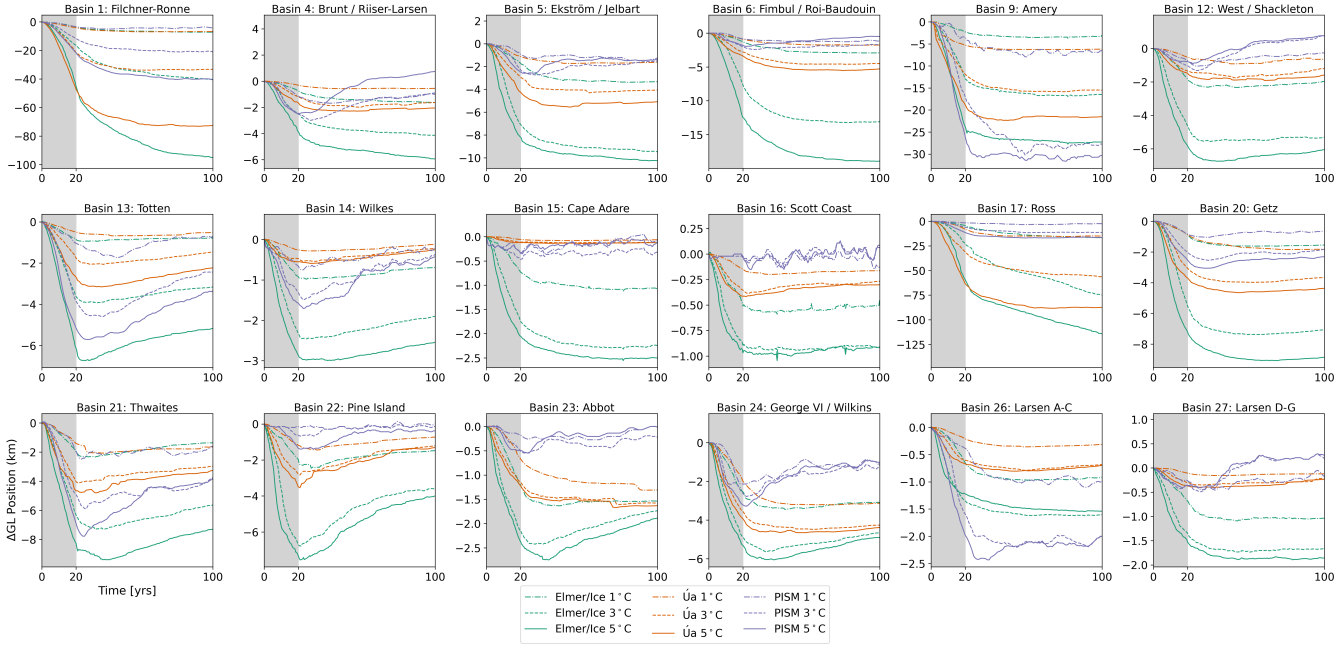

Figure S12. Change in grounding line position for individual drainage basins. Results are shown for all three models and all perturbation experiments with respect to their control experiments.

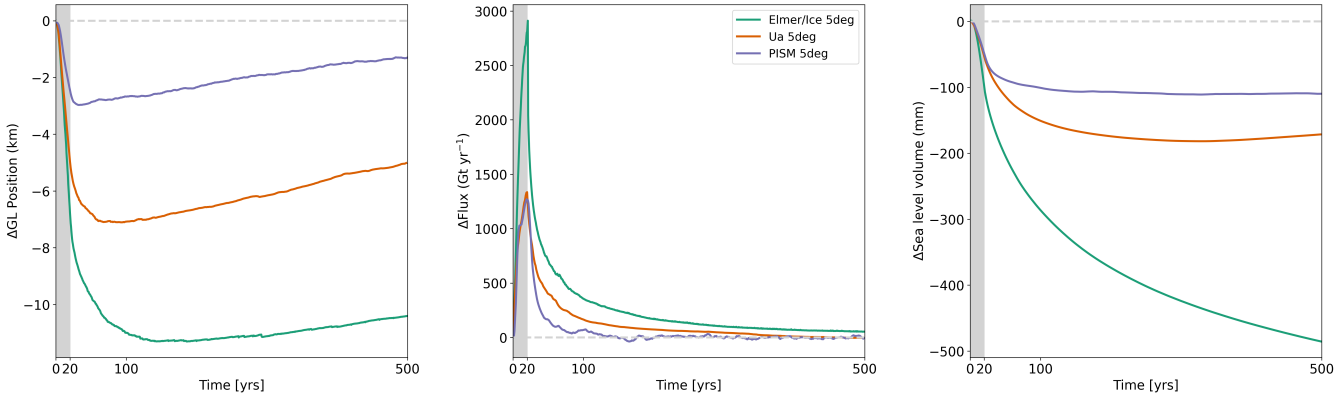

Figure S13. Antarctic-wide results extended to 500 years for all three models for the 5 °C perturbation experiment.

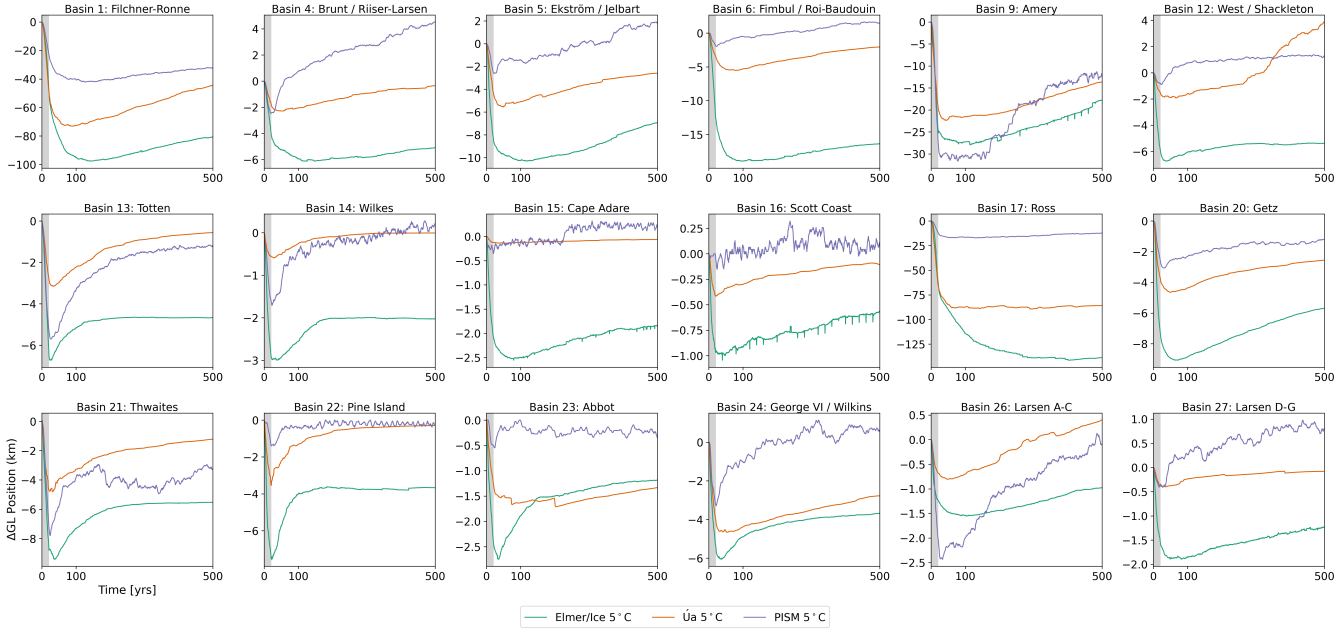

Figure S14. Change in grounding line position for individual drainage basins. Results are shown for all three models for the 5 °C perturbation experiment.

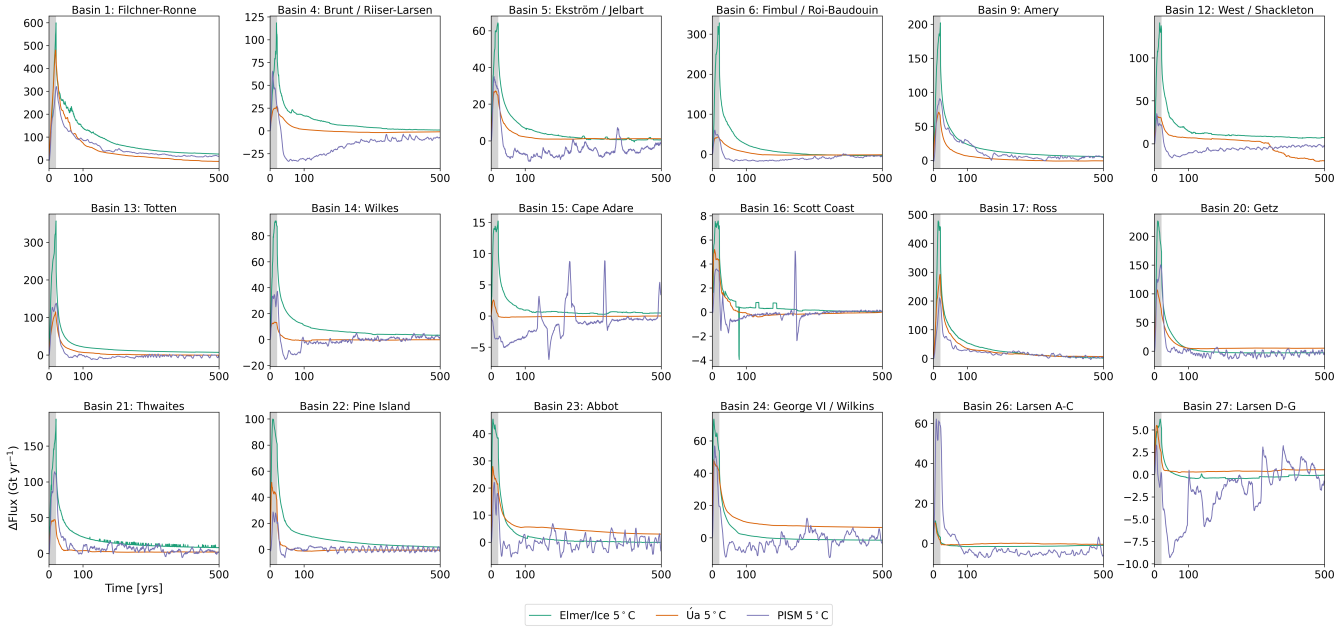

Figure S15. Change in grounding line flux for individual drainage basins. Results are shown for all three models for the 5 °C perturbation experiment.

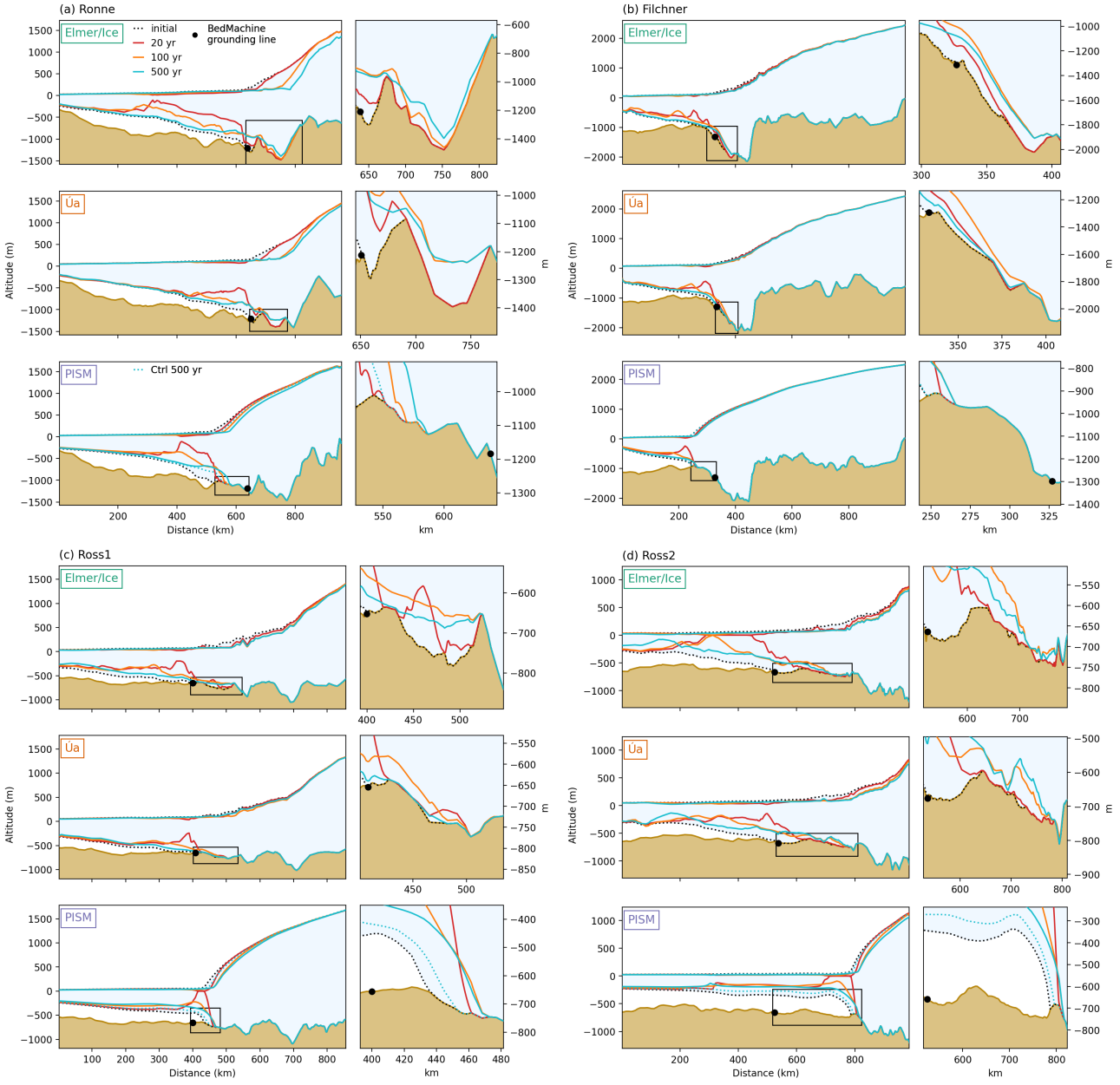

Figure S16. Profiles of the Ronne, Filchner, and Ross ice shelves for the three models at different time intervals during the 5 °C experiment. Shown are the ice-sheet geometries of the initial state (dotted line filled with light blue), at the end of the perturbation (red line), after 80 years of release (orange line), and after 500 years (cyan line). The small panels show a zoom into the grounding line zone marked by the black squares. The resolution of each profile depends on the model resolution. Profile locations are shown in Fig. 2.

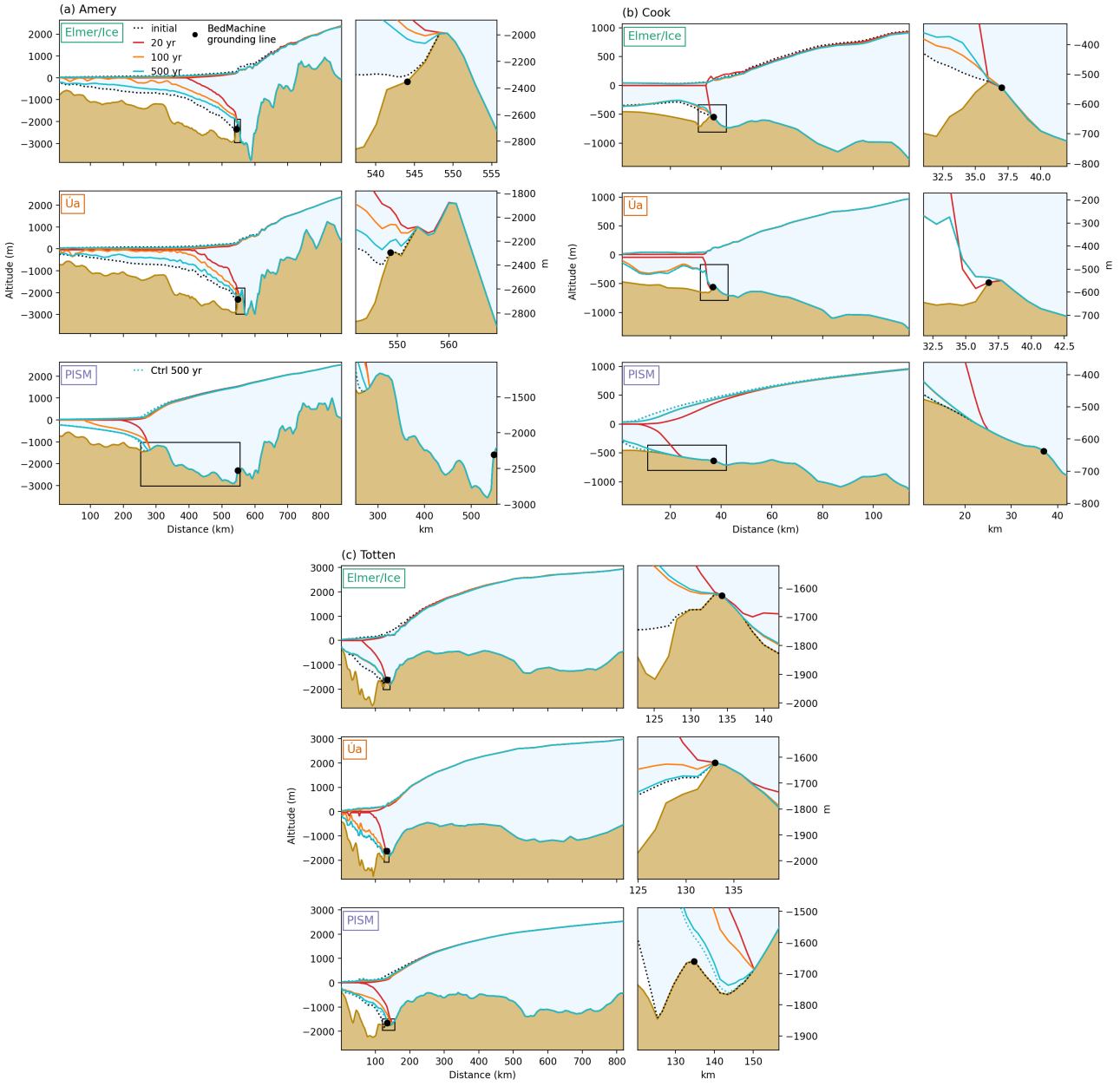

Figure S17. Profiles of the Amery, Cook, and Totten ice shelves for the three models at different time intervals during the 5 °C experiment. Shown are the ice-sheet geometries of the initial state (dotted line filled with light blue), at the end of the perturbation (red line), after 80 years of release (orange line), and after 500 years (cyan line). The small panels show a zoom into the grounding line zone marked by the black squares. The resolution of each profile depends on the model resolution. Profile locations are shown in Fig. 2.